A

Phenotypes associated with targeted expression of H3.3K27M, H3.3K36M and H3.3 WT.

Promoter	Lineage	Phenotype		
		K27M	***K36M***	***WT***
Act5C	ubiquitous	larval-pupal lethal	larval lethal	no phenotype
ey	**eye discs**	**small eyes**	**small eyes**	**no phenotype**
robo2	leg discs	adult lethal, leg deformity	adult lethal, leg deformity	no phenotype
robo1	imaginal discs	leg deformity	leg deformity	no phenotype
en	wing discs	pupal lethal	pupal lethal	no phenotype
ptc	anterior-posterior axis imaginal discs	leg and wing deformity	anterior cross vein missing	no phenotype
c179	muscles and wing discs	pupal lethal	pupal lethal	no phenotype
Mef2	muscles	pupal lethal	pupal lethal	no phenotype
CG25C	haemocytes	increased haemocyte numbers (–4 x 10^7cells/ml)	increased haemocyte numbers (–4 x 10^7 cells/ml)	no phenotype (–2 x 10^7 cells/ml)
elav	neurons	no phenotype	no phenotype	no phenotype
slit	MGC and MP1 neurons	pupal lethal	pupal lethal	no phenotype
repo	glia	pupal lethal	pupal lethal	no phenotype
gcm	glia	no phenotype	no phenotype	no phenotype
crol	CNS	pupal lethal	larval-pupal lethal	no phenotype
ama	CNS and imaginal discs	leg weakness (80-68% climbing ability)	leg weakness (88-85% climbing ability)	no phenotype (96-90% climbing ability)
appl	CNS and imaginal discs	larval-pupal lethal	larval-pupal lethal	no phenotype
tkk	CNS, ovary and testis	pupal lethal	pupal lethal	no phenotype

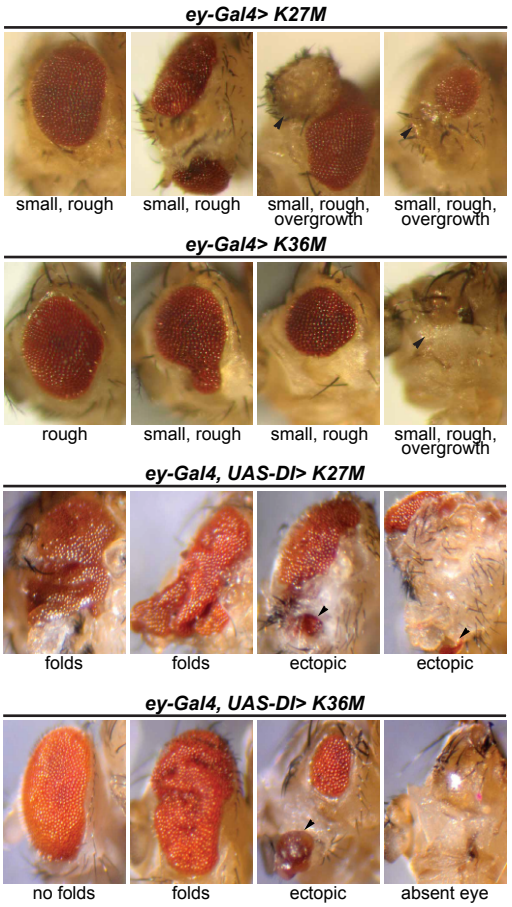

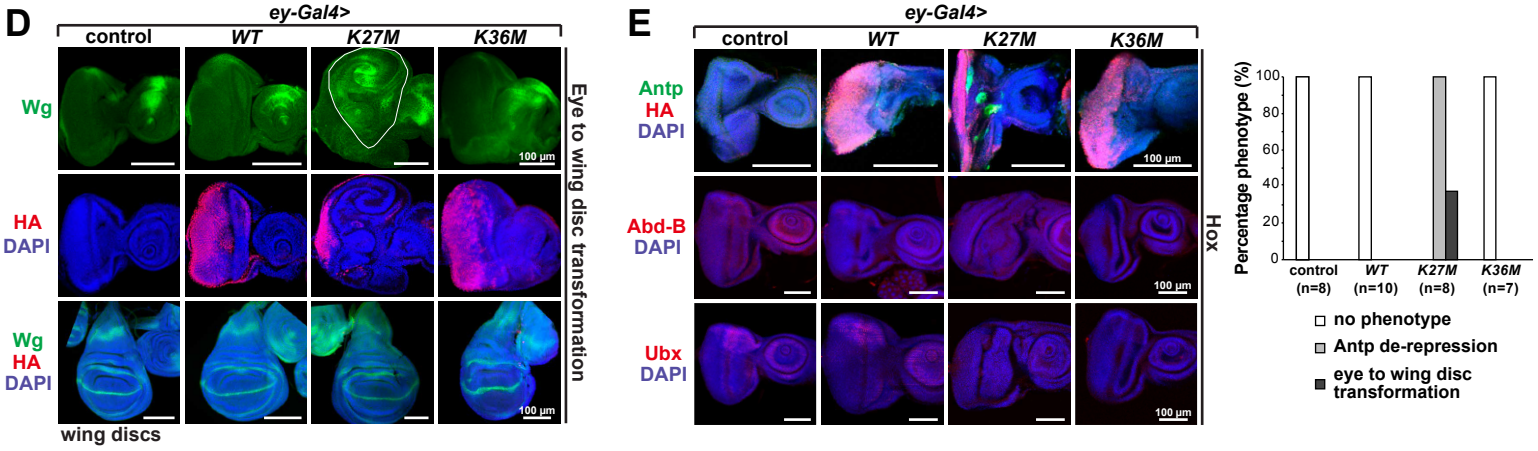

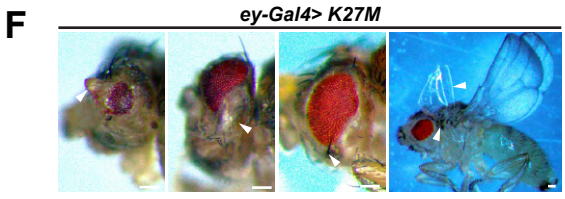

Figure S1. Detailed analysis of eye phenotypes in mutant histone H3.3 expressing flies, Related to Figure 1.

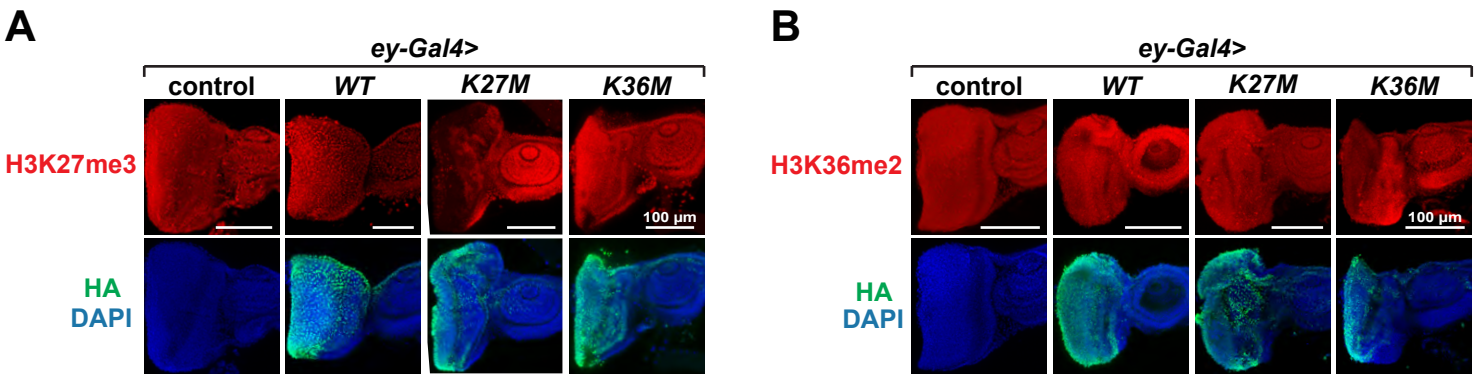

Figure S2. Quantification of global changes in histone marks in mutant and wild-type histone H3.3 expressing flies, Related to Figure 2.

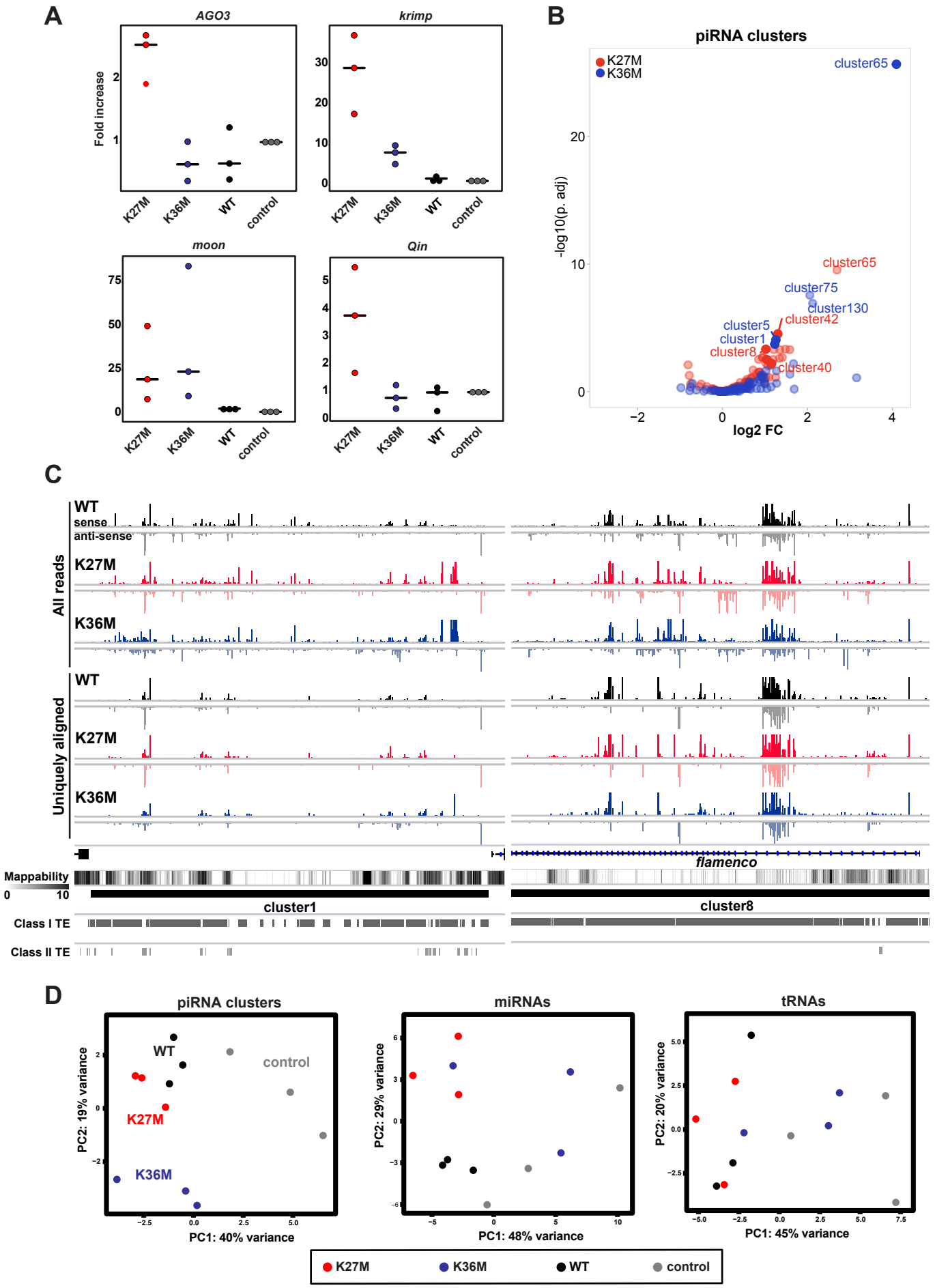

Figure S3. K-to-M mutations result in induction of piRNA genes, Related to Figure 3.

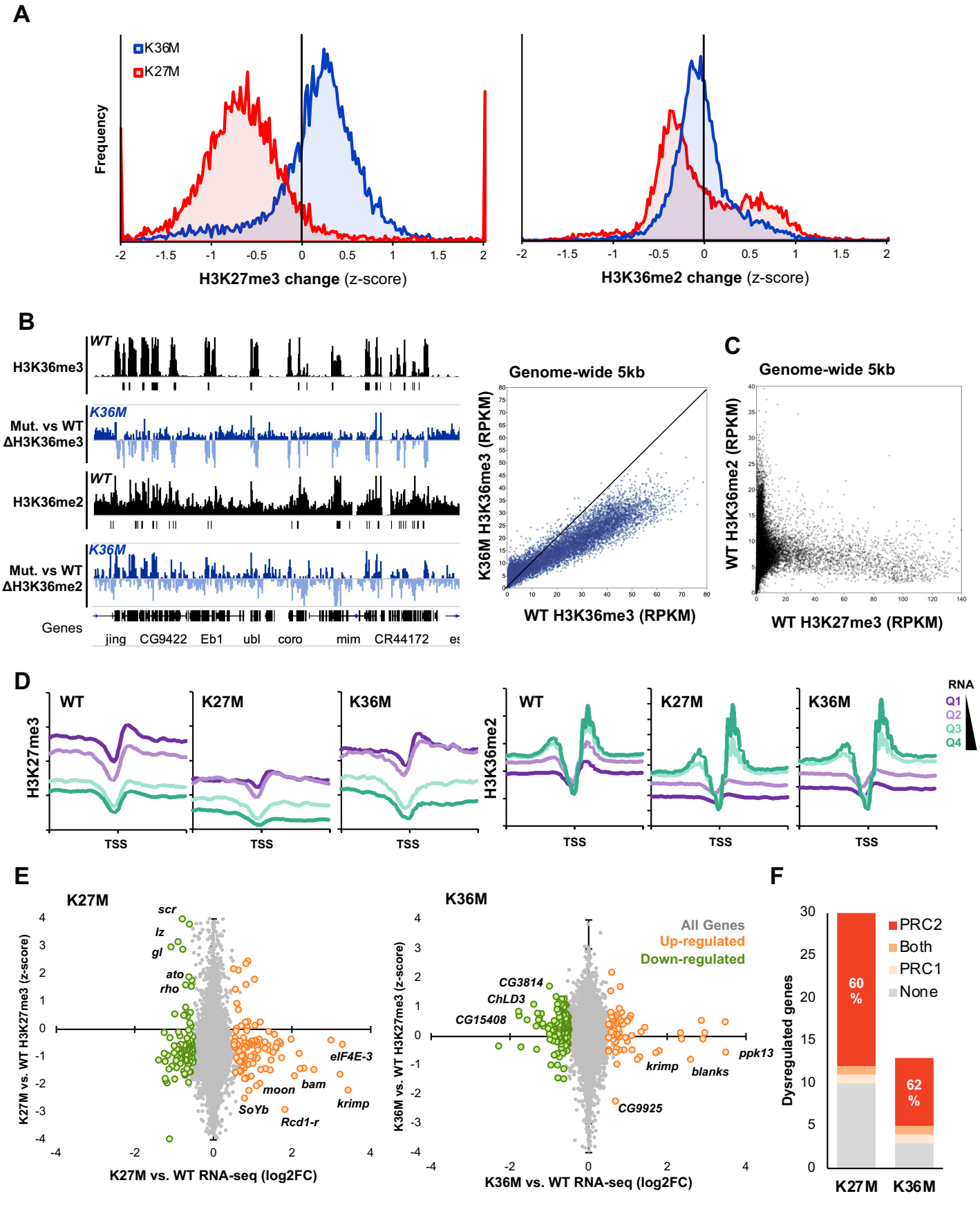

Figure S4. H3.3K27M and H3.3K36M perturb global H3K27me3/H3K36me2 landscape, Related to Figure 4.

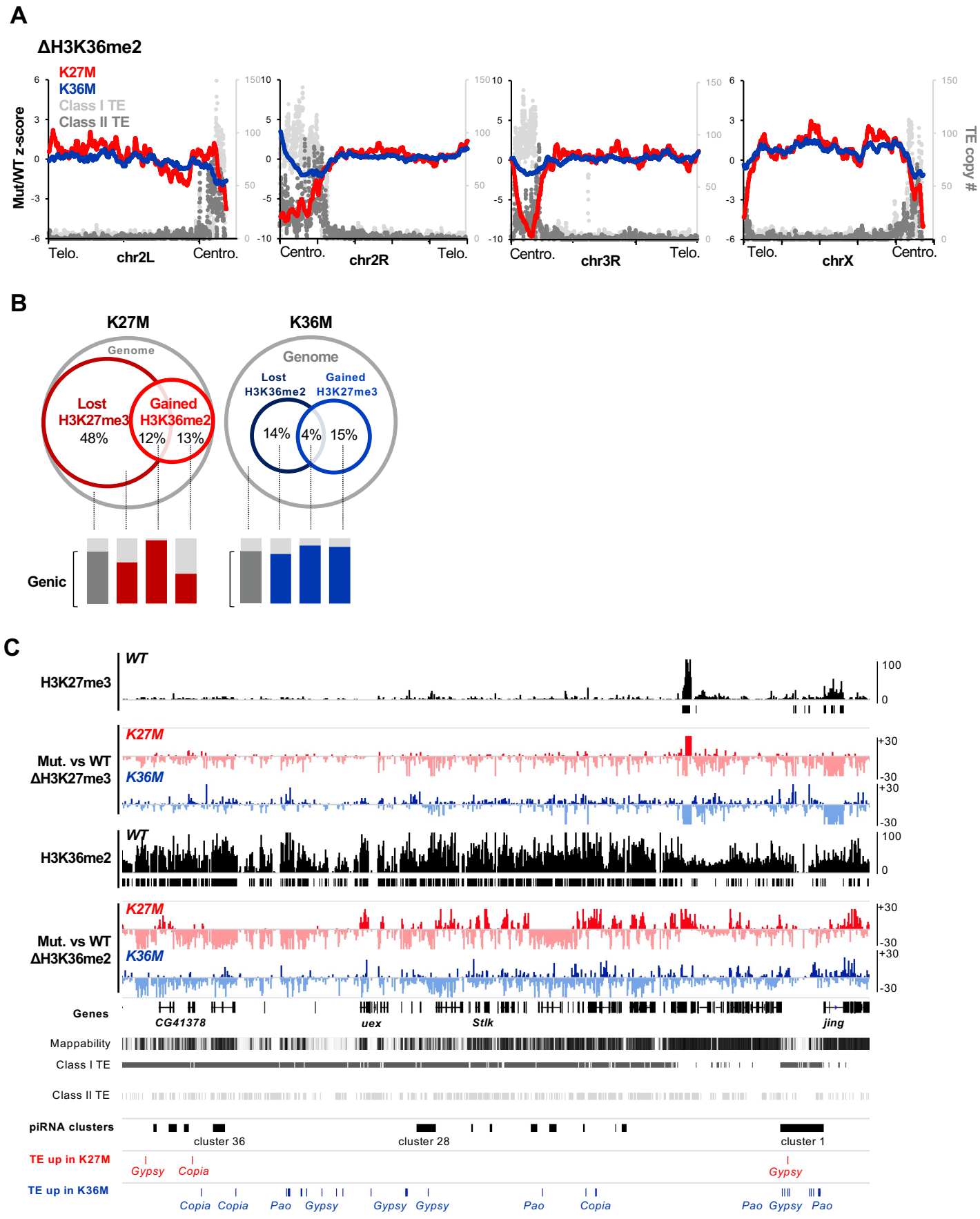

Figure S5. H3.3K27M and H3.3K36M redistribute H3K36me2 away from repetitive regions, Related to Figure 4.

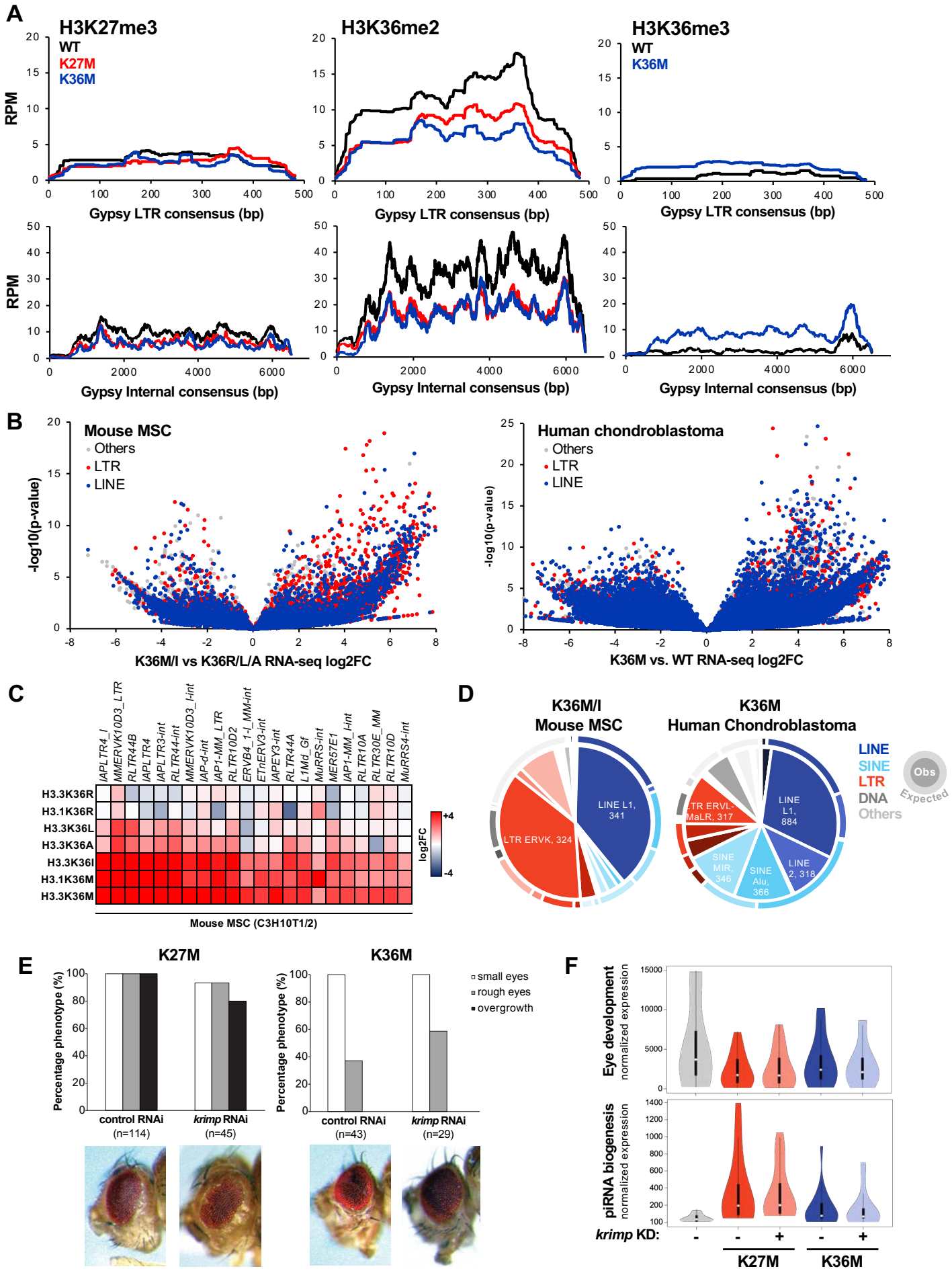

Figure S6. H3.3K27M and K36M de-repress transposable elements in flies, Related to Figure 5.

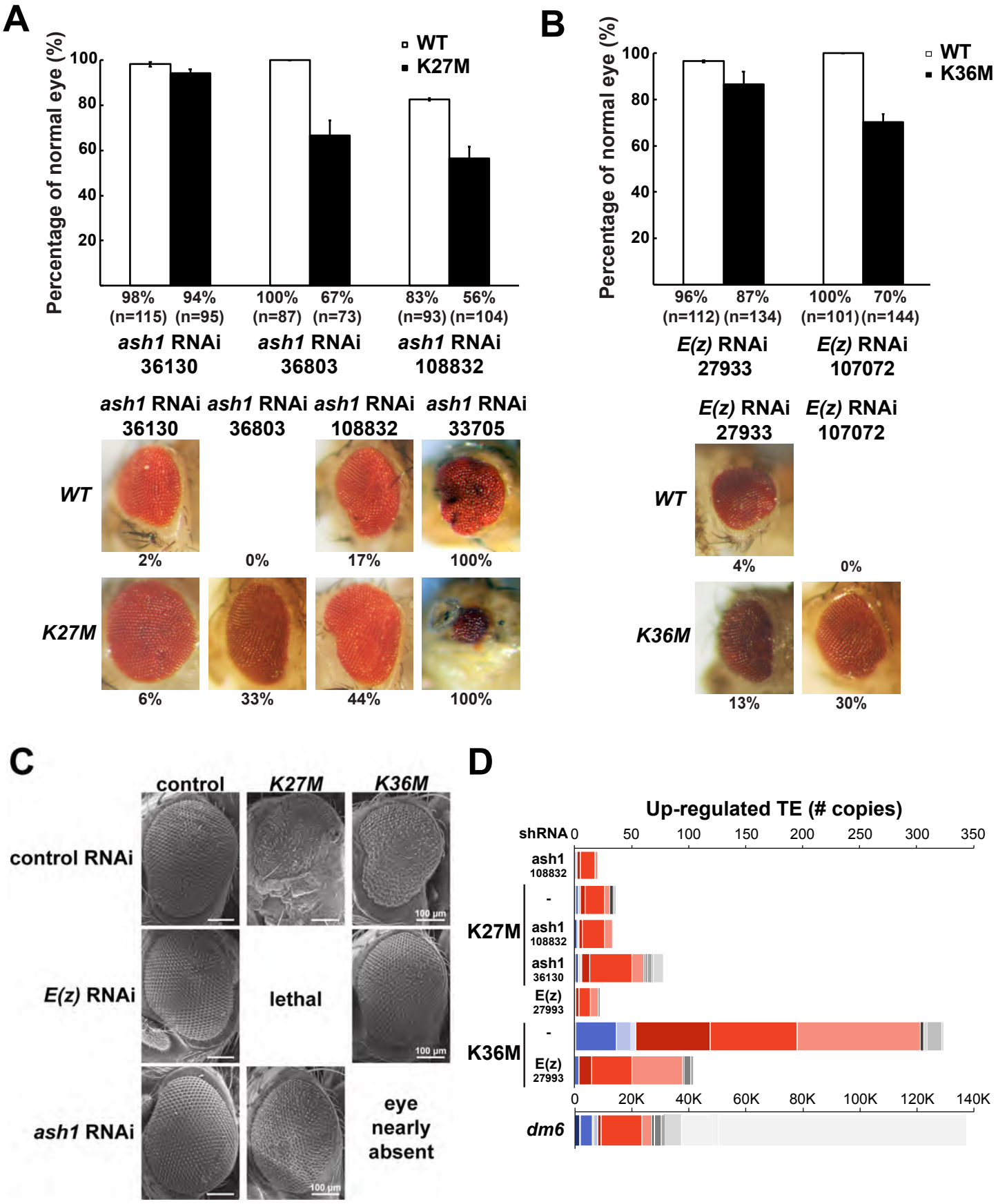

Figure S7. shRNA-mediated knockdown of the H3K27 methyltransferase E(z) and the H3K36 methyltransferase ash1 restores normal eye development in mutant H3.3 expressing eye discs, Related to Figure 6.

Supplemental Figure Legends

Figure S1. Detailed analysis of eye phenotypes in mutant histone H3.3 expressing flies, Related to Figure 1.

(A) Phenotypes associated with targeted expression of H3.3K27M, H3.3K36M and H3.3 WT. (**B**) Expression of H3.3K27M and H3.3K36M in eye imaginal discs resulted in a small/rough eye phenotype with a variation regarding size of compound eyes and tumorous growth of additional head and eye tissue (black arrowheads). The eye phenotype upon H3.3K27M expression was notably more severe as compared to H3.3K36M expression. (**C**) Range of eye phenotypes upon expression of H3.3K27M or H3.3K36M in a sensitized *ey-Gal4, UAS-Dl* background. Expression of H3.3K27M or H3.3K36M resulted in tumorous eyes with variable severity including overgrowth, hyperplastic tissue with folds, metastasis (black arrowheads) or complete loss of eye tissue. **(D)** Immunofluorescence staining for Wg, a ligand of the Wnt/Wg signaling pathway. In approximately one third of eye discs expressing H3.3K27M, expression of Wg shifts to a wing-like pattern in the dorsal part of the eye disc as marked by the white outline. Scale bar 100µm. **(E)** Immunofluorescence staining for the Hox proteins Antp, Abd-B, and Ubx in H3.3K36M, H3.3K27M and H3.3 WT overexpressing eye discs. Transgene expression is visualized by HA staining. There is no de-repression of Abd-B or Ubx in histone H3 mutant expressing discs visible. **(F)** Micrographs of adult eyes illustrating ectopic tissues observed in the eye and head region of H3.3K27M expressing animals (*ey-Gal4*) including leg-like structures, thoracic bristles and an extra pair of wings (white arrows).

Figure S2. Quantification of global changes in histone marks in mutant and wild-type histone H3.3 expressing flies, Related to Figure 2.

(**A**) Immunofluorescence staining for H3K27me3 or (B) H3K36me2 combined with histone transgene expression (HA staining) in Gal4 control, H3.3 WT, H3.3K27M and H3.3K36M overexpressing eye discs.

Figure S3. K-to-M mutations result in induction of piRNA genes, Related to Figure 3.

(**A**) Dot plots showing qPCR results from three independent experiments validating that *krimp*, *moon*, *AGO3*, and *qin* RNA levels are elevated in H3.3K27M eye discs, and that *krimp* and *moon* RNA levels are elevated in H3.3K36M eye discs. The y-axis shows fold increase relative to *yw* controls. (**B**) Differential expression analysis of piRNA clusters following small RNAseq between H3.3K27M or H3.3K36M compared to baseline control. **(C)** Genome browser snapshot depicting piRNA expression at *cluster 1* (left) and *flamenco/cluster 8* (right) in H3.3WT (black), H3.3K27M (red), and H3.3K36M mutants (blue). Upper panel: all aligned reads in the sense (positive, darker) and anti-sense (negative, lighter) orientation. Lower panel: uniquely aligned (mapQ $\geq$ 1) reads. (**D**) Principal component analysis of the smRNA-seq data, using as features expression of piRNA clusters (left), microRNA genes (middle), or tRNAs (right).

Figure S4. H3.3K27M and H3.3K36M perturb global H3K27me3/H3K36me2 landscape, Related to Figure 4.

(A) Histogram of genome-wide H3K27me3 (left) and H3K36me2 (right) changes in H3.3K27M and H3.3K36M mutant flies. Positive z-score indicate gain of the mark in mutant vs. H3.3 WT flies. **(B)** Left: browser snapshot of H3K36me3 and H3K36me2 loss in H3.3K36M eye disc compared to H3.3WT. Right: genome-wide 5kb quantification of H3K36me3 in H3.3 WT vs. H3.3K36M. **(C)** Scatterplot depicting genome-wide anti-correlation between H3K27me3 and H3K36me2 in H3.3 WT eye disc. **(D)** Metagene plot depicting H3K27me3 and H3K36me2 level in relation to transcriptional activity in H3.3 WT, H3.3K27M, and H3.3K36M. Genes were stratified into 4 quartiles based on expression in H3.3 WT (Q1 being silenced and Q4 being highly transcribed), and H3K27me3/H3K36me2 enrichment (RPKM) were plotted in 5 kilobase window centered on the transcription start site. **(E)** Scatterplot depicting the relationship of gene expression change vs. H3K27me3 at all annotated promoters. **(F)** Overlap of differentially expressed genes

with genes deregulated upon loss-of-function of PRC1 or PRC2 in the *Drosophila* eye (Loubiere et al., 2016).

Figure S5. H3.3K27M and H3.3K36M redistribute H3K36me2 away from repetitive regions, Related to Figure 4.

(A) Smoothed line plot depicting H3.3K27M- or H3.3K36M-mediated H3K36me2 change in relation to transposable element (TE) copy numbers on autosomes and chromosome X. **(B)** Venn diagram of genomic bins showing concurrent H3K27me3-loss/H3K36me2-gain in H3.3K27M (left), and reciprocally H3K36me2-loss/H3K27me3-gain in H3.3K36M (right). Below, the percentage of bins falling into genic vs. intergenic region in each category. Note enrichment of genic bins in the intersection of H3K27me3/H3K36me2 change in both mutants. **(C)** Genome browser snapshot of pericentromeric region of chr2R, showing localization of up-regulated TE observed in H3.3K27M and H3.3K36M flies. Black boxes: WT H3K27me3 and WT H3K36me2 called peaks.

Figure S6. H3.3K27M and K36M de-repress transposable elements in flies, Related to Figure 5.

(A) Alignment of H3K27me3 and H3K36me2/3 at Gypsy LTR (upper panels) and internal (lower panels) consensus sequence in H3.3 WT (black), K27M (red), and K36M (blue). (**B**) Volcano plot depicting K36M-mediated transcriptional dysregulation in repetitive sequences in murine mesenchymal stem cells, or MSCs (left), and human primary chondroblastoma (right). Each dot represents an individual copy of repeat, and red dots represent individual LTR elements while blue dots depict LINEs. **(C)** Heatmap depicting TE de-repression in panel of K36 mutants relative to H3.3WT-expressing MSCs. **(D)** Pie chart depicting number and diversity of repeat copies showing significant up-regulation ($log2FC > 2$, $FDR < 0.05$) in murine MSCs and human chondroblastoma. Outer ring: copy number of each repeat class in the respective mouse (mm10) and human (hg19) genomes. **(E)** The *krimp* shRNA strain BDSC#35230 was tested regarding its potential to rescue the eye phenotype compared to H3.3K27M or H3.3K36M expression combined with control RNAi (mCherry BDSC#35785) knockdown. Micrographs (lower panel) show representative images of H3.3K27M/*krimp* RNAi (small, rough with overgrowth) and H3.3K36M/*krimp* RNAi (small, not

rough) expressing flies compared to control flies. Eye phenotypes of H3.3K27M and H3.3K36M expressing flies are scored according to the following criteria: small eyes, rough eyes and overgrowth. Note that there was no major rescue detected upon *krimp* knockdown. **(F)** Violin plot representing normalized expression score for eye developmental genes and germ cell/piRNA genes in *krimp*-KD H3.3K27M and H3.3K36M flies, relative to mCherry KD controls.

Figure S7. shRNA-mediated knockdown of the H3K27 methyltransferase E(z) and the H3K36 methyltransferase ash1 restores normal eye development, Related to Figure 6.

(A) Three independent *ash1* shRNA strains were tested regarding their potential to rescue the eye phenotype observed upon *ey*>H3.3K27M expression (BDSC ID 36130: 94.39% rescue, sem: 1.56, n=95; VDRC ID 108832: 56.54% rescue, sem: 5.30, n=104; BDSC ID 36803: 66.70% rescue, sem: 6.67, n=73). Micrographs (right panel) show H3.3K27M/*ash1* RNAi expressing flies which were not completely rescued, as well as H3.3 WT/*ash1* RNAi expressing flies exhibiting an eye phenotype (BDSC ID 36130: 1.79% eye phenotype, sem: 1.03, n=115; VDRC ID 108832: 17.44% eye phenotype, sem: 0.59, n=93; BDSC ID 36803: 0% eye phenotype, n=87). (**B**) Two independent *E(z)* shRNA strains were tested regarding their potential to rescue the eye phenotype observed upon eyeless-specific H3.3K36M expression (BDSC ID 27993: 86.62% rescue, sem: 5.47, n=134; VDRC ID 107072: 70.29% rescue, sem:3.29, n=144). Micrographs (right panel) show H3.3K36M/*E(z)* RNAi expressing flies which were not completely rescued, as well as H3.3 WT/*E(z)* RNAi expressing flies exhibiting an eye phenotype (BDSC ID 27993: 3.48% eye phenotype, sem: 0.54, n=112; VDRC ID 107072: 0% eye phenotype, n=101). (**C**) SEM micrographs of adult eyes illustrating modifier effects of *E(z)* and *ash1* knockdown on *eyeless*>H3.3K27M and *ey*>H3.3K36M flies. Expression of either *E(z)* or *ash1* shRNA alone has no significant phenotype. (**D**) Number of transposon elements significantly up-regulated (log2FC > 0, FDR < 0.05) in *ash1*-rescued K27M and *E(z)*-rescued K36M, compared to *ash1*-KD alone, *E(z)*-KD alone, and mCherry RNAi negative control. Below, copy number of each repeat class in *dm6*.

Table S3: Differential expression analysis of piRNA biogenesis genes in eye imaginal discs expressing H3.3K27M compared to *yw* controls, Related to Figure 3.

		Ensembl_ID	Symbol_ID	log2FoldChange	*P*-value adjusted
piRNA biogenesis	PIWI proteins	FBgn0000146	aub	0.2446	0.599771
		FBgn0250816	AGO3	1.1092	5.06E-08
		FBgn0004872	piwi	0.7686	0.001316
	TDRD proteins	FBgn0003891	tud	0.0000	0.999787
		FBgn0031401	papi	0.2042	0.015961
		FBgn0263974	qin	1.7866	1.91E-22
		FBgn0033921	tej	0.1767	0.727586
		FBgn0003483	spn-E	-0.3718	0.056024
		FBgn0000928	fs(1)Yb	1.0245	2.26E-06
		FBgn0037205	BoYb	1.6285	5.97E-13
		FBgn0051755	SoYb	2.8846	4.8E-166
		FBgn0263143	vret	0.2275	0.20485
		FBgn0034098	krimp	3.8891	6.2E-224
		FBgn0086908	egg	0.0228	0.901081
	Other nuage proteins	FBgn0041164	armi	0.0760	0.471933
		FBgn0262526	vas	0.6323	0.007611
		FBgn0016034	mael	1.3151	7.06E-12
		FBgn0261266	zuc	0.3371	0.193764
		FBgn0267347	squ	0.2220	0.009817
		FBgn0003401	shu	0.3056	0.096796
	Heterochromatin piRNA transcription	FBgn0030373	CG12721/moon	1.9618	8.04E-18
		FBgn0086251	del	1.5923	3.46E-77
	nuclear proteins involved in piRNA biogenesis	FBgn0014189	Hel25E/uap56	0.1017	0.054590
		FBgn0004400	rhi	0.1037	0.871447
	pole plasm	FBgn0003165	pum	-0.1904	0.307085
		FBgn0003520	stau	-0.1109	0.397707
		FBgn0016053	pgc	0.1206	NA
		FBgn0003015	osk	-0.4840	**NA**
		FBgn0002962	nos	0.9065	0.000523

Table S6: RNAi strains for genetic modifier screen including PRC1, PRC2 members, lysine methyltransferases and candidates from the piwi-interacting RNA (piRNA) pathway, Related to Figure 5-6.

no.	CG no.	Fruit Fly gene name	Human ortholog	VDRC ID	BDSC/DGRC ID	UAS #	Vector
1	CG6502	E(z)	EZH2		27993	10	VALIUM 10
2	CG6502	E(z)	EZH2	107072		10	KK
3	CG14941	Esc	EED	5690		10	GD
4	CG5202	Escl	EED	49982		10	GD
5	CG8013	Su(z)12	SUZ12		33402	10	VALIUM 20
6	CG4236	Caf1-55	RBBP4	26455		10	GD
7	CG9397	Jing	AEBP2		55633	10	VALIUM 20
8	CG8887	ash1	ASH1L		36130	10	VALIUM 10
9	CG8887	ash1	ASH1L		36803	10	VALIUM 22
10	CG8887	ash1	ASH1L	108832		10	KK
11	CG1716	Set2	SETD2		55221	10	VALIUM 22
12	CG5595	Sce	RING1, RNF2	106328		10	KK
13	CG3886	Psc	BMI1	30587		10	GD
14	CG3905	Su(z)2	BMI1	50368		10	GD
15	CG32443	Pc	CBX6, CBX8		33622	10	VALIUM 20
16	CG9495	Scm	SCMH1	109597		10	KK
17	CG18412	ph-p	PHC3	100811		10	KK
18	CG3895	ph-d	PHC2		63018	10	VALIUM 20
20	CG5640	Utx	KDM6A/B		34076	10	VALIUM 20
21	CG11033	kdm2	KDM2A/B		31360	10	VALIUM 1
22	CG4976	NSD	NSD1/2/3		34033	10	VALIUM 20
23	CG15707	Krimp	TDRD1		35230	10	VALIUM 22

Table S7: Patched-specific modifier screen, Related to Figure 6.

RNAi tested	*wing defects in K27M expressing flies*	*leg defects in K27M expressing flies*	*Rescue of K36M wing phenotype (ACV loss)*
mCherry control	*80% ± 7*	*98% ± 4*	
E(z)	*100%*	*100%*	
Esc	*100%*	*100%*	
Escl	*93%*	*100%*	
Su(z)12	*100%*	*100%*	
Caf1-55	*77%*	*100%*	
Jing	***lethal***	***lethal***	
Psc	*95%*	*100%*	
Su(z)2	*92%*	*100%*	
Sce	*100%*	*100%*	
Pc	*100%*	*100%*	
Ph-p	*100%*	*100%*	
Ph-d	**54% ± 4**	**67% ± 16**	*n.d.*
Scm	**lethal**	**lethal**	
ash1	**31.0% ± 11**	**58.5 %± 8**	
Nsd	77% ± 8	100%	
Set2	91%	100%	
kdm2	*85.0% ± 2*	*95% ± 1*	
Utx	*92%*	*100%*	

Table S8: Modifier screen including PRC1, PRC2 members and lysine methyltransferases, Related to Figure 6.

RNAi tested	*slit*-GAL4> K36M	*Act5C*-GAL4> K36M	*ey*-Gal4> K27M	*ey*-GAL4> K36M
mCherry control	pupal lethality	pupal lethality, pupation defects	rough, small eyes	rough, small eyes
E(z) 27993	viability: 89.0% ± 6.4	no pupation defects	lethal	positve shift
Esc	no shift	larval lethal	no shift	no shift
Escl	no shift	larval lethal	no shift	no shift
Su(z)12	no shift	no shift	lethal	negative shift*
Caf1-55	no shift	larval lethal	lethal	lethal
Jing	larval lethal	larval lethal	lethal	lethal
Psc	no shift	larval lethal	no shift	no shift
Su(z)2	no shift	larval lethal	78% lethal	94% lethal
Sce	no shift	larval lethal	lethal	lethal
Pc	no shift	larval lethal	91% lethal	93% lethal
Ph-p	no shift	no shift	no shift	no shift
Ph-d	no shift	no shift	no shift	no shift
Scm	no shift	no shift	lethal	lethal
ash1 108832	no shift	no shift	positve shift	99% lethal
NSD	no shift	no shift	no shift	no shift
Set2	no shift	no shift	no shift	no shift
kdm2	no shift	no shift	no shift	no shift
UTX	no shift	no shift	no shift	no shift

* Sex specific differences: Su(z)12 negative shift only in females

Table S9: Additional *ash1* and *E(z)* RNAis tested, Related to Figure 6.

RNAi tested	*slit*-GAL4> K36M	*Act5C*-GAL4> K36M	*ey*-Gal4> K27M	*ey*-GAL4> K36M
mCherry control	pupal lethality	pupal lethality, pupation defects	rough, small eyes	rough, small eyes
E(z)107027	no shift	no shift	**lethal**	**positve shift**
ash1 36803	no shift	no shift	**positve shift**	**negative shift**
ash1 36130	no shift	no shift	**positve shift**	no shift